JOURNAL OF GEOPHYSICAL RESEARCH, VOL. 102, NO. B7, PAGES 14,883–14,897, JULY 10, 1997

Electric potential changes associated with slip failure of granite: Preseismic and coseismic signals

Shingo Yoshida, Makoto Uyeshima,[1] and Masao Nakatani[2]

Earthquake Research Institute, University of Tokyo, Tokyo, Japan

Abstract. Electric potential changes were measured for stick-slip events in granite samples with a three-block direct shear arrangement at 8 MPa normal stress. Two electrodes were mounted on the left- and right-hand blocks, and the electric potential difference between each electrode and the ground was measured with a high input impedance recording system of frequency range from DC to 100 Hz. As well as coseismic electric signals of about 1.5 V which appeared the moment of the dynamic slip event, preseismic signals were detected just before the slip event. The coseismic signal rises stepwise with opposite polarities at the two electrodes and exponentially decays with a time constant of ε/s, where ε is the permittivity and s is the conductivity of the rock sample. We conducted a simple test of rapid stress drop without slipping and observed almost the same electric signal as the coseismic signal. This suggests that the electric signal is generated by the piezoelectric effect. We proposed a generation model based on the piezoelectric effect and the resultant relaxation process and obtained a theoretical frequency response, which is in agreement with experimental data. The preseismic signal appears about 2-3 s before the dynamic event with an amplitude of about 50 mV. The local strains along two sliding surfaces were also measured to monitor the growth of the rupture nucleation zone. When the growth of the rupture nucleation zone occurred on the left sliding surface, a clear preseismic signal was detected at the electrode mounted on the left granite block. When the growth occurred on the right-hand surface, a signal was detected at the electrode on the right block. This shows that the preseismic electric signal is caused by stress change in the rupture nucleation zone. These preseismic and coseismic signals were also detected with an antenna, which was placed away from the sample surface.

1. Introduction

Seismic electric signals (SES) have been used as precursors to earthquakes for the VAN (Varotsos, Alexopoulos, and Nomicos) method of earthquake prediction in Greece [e.g., *Varotsos and Alexopoulos*, 1984a,b], but the signal generation mechanisms are not sufficiently understood. There have been many laboratory studies on electric signals associated with rock fracture including electromagnetic emissions (EME). Some studies have suggested that the electric signals are produced mainly by the piezoelectric effect of quartz [e.g., *Nitsan*, 1977; *Warwick et al.*, 1982; *Ogawa et al.*, 1985; *Lockner et al.*, 1986; *Yoshida et al.*, 1994], and others have proposed different mechanisms such as the electrokinetic effect, contact electrification (or separation electrification), motion of rock fragments with charged surfaces, and point defects [e.g., *Mizutani et al.*, 1976; *Cress et al.*, 1987; *Yamada et al.*, 1989; *Enomoto and Hashimoto*, 1992; *Hadjicontis and Marvomatou*, 1994]. In the zone where actual earthquake occurs, more than one mechanism may work at the same time. To understand the electric phenomena in the field and to infer which mechanism dominates, it is important to make clear the specific characteristic of electric signal due to each possible mechanism through experimental results. We must make a quantitative model for each individual mechanism and describe it in terms of physical parameters. If more than one mechanism operates in the field, understanding of the frequency characteristics is essential to interpret the observed signals and divide them into separate components. In the present paper, as a first step to such an approach, we will attempt to make clear the mechanisms due to the piezoelectric effect, using a dry granite sample to avoid contamination from the electrokinetic effect. We focus on the piezoelectric effect because there is no doubt that it causes electric field change, although it is not obvious whether the amplitude is observable or not. Most of previous laboratory studies on piezoelectricity have not measured a DC component, partly because an extremely high input impedance measuring system is needed to measure the DC component of the electric signal from dry rock. In the present paper, measurements in a broadband frequency range, including a DC component, will be done because one of our interests concerns the variation of the DC component as measured in the VAN method.

Some investigators expect the electric signal is useful for earthquake prediction. Recently, our understanding of the rupture nucleation process before the main rupture has progressed through experimental, theoretical, and observational studies. If we find some precursory signal related to the nucleation process, it would not be difficult to understand a causal relationship between such a precursory signal and the earthquake. Therefore one effective approach on precursors is to observe what happens during the rupture nucleation process in laboratory experiments. In the present paper, we describe a

[1]Also at Institute of Theoretical Geophysics, University of Cambridge, Cambridge, England.

[2]Now at the Lamont-Doherty Earth Observatory of Columbia University, Palisades, New York.

Paper number 97JB00729.
0148-0227/97/97JB-00729$09.00

direct shear experiment where slip failure occurs on simulated fault planes. Rupture nucleation growth on the weak surface is well understood [e.g., *Scholz et al.*, 1972; *Dieterich*, 1979; *Ohnaka*, 1992; *Shibazaki and Matsu'ura*, 1992], and actual earthquakes are considered to occur along weak surfaces such as active fault planes or plate boundaries.

2. Experimental Procedure

Using a biaxial servo-controlled loading apparatus, frictional experiments were carried out in a three-block direct shear configuration where a central granite block (5×10×14 cm) was sandwiched by two outer granite blocks (5×5×14 cm), as shown in Figure 1. Each of the two sliding surfaces had an area of about 5×14 cm^2. The sliding surfaces were ground flat with a reciprocating surface grinder and then were lapped with 1000 mesh silicon carbide abrasive. In this way we produced relatively smooth surfaces for which the critical displacement D_c was small enough to lead to stick slip events. As is well known, dynamic instability resulting in sudden slip across the sliding surfaces, with a sudden stress drop, can occur repeatedly depending on the stiffness of the loading machine and the critical displacement D_c of the rock sample [e.g., *Scholz*, 1990]. The motion of the vertical ram was servo-controlled at a displacement rate of 0.4×10^{-6} m/s throughout the experiment using a high-speed servo-control valve, and normal stress applied on the sliding surfaces was held constant (8 MPa) by a servo-controlled horizontal ram. The experiments were carried out at room temperature without any control on water content in the rock sample except that we dried the samples in an oven after lapping them.

The granite blocks were electrically isolated from the ground by alumina blocks with a nominal specific resistivity $>10^{16}$ Ω m. Two silver electrodes, about 1 cm in diameter, were mounted on the left and right granite blocks, and the electrical potential difference between each electrode and the ground was measured using Keithley 617 and 6517 electrometers with an input impedance in excess of 10^{14} Ω and a frequency range of DC to 100 Hz. Electrical leads of Teflon coaxial cable were used from the electrode to the electrometer to reduce noise. The electric potentials at the two electrodes were digitally recorded at a sampling frequency of 2 kHz in most tests, but the sampling frequency was varied up to 1 MHz, depending on the aim of the test using different amplifiers with a broad frequency range as described in section 3.5. To observe the local shear strain as a function of time and position along the sliding surface, five strain gauges were mounted along each sliding surface. Ten channels of shear strains were measured in total. The strain gauges were positioned 5 mm from the sliding surface at 25 mm intervals. The strain gauges and the electrode were mounted on opposite sides of the sample to avoid the interference between the electrodes and strain gauges. The strain signal was filtered out above 1 kHz when the sample frequency was 2 kHz. In addition to the two electric potentials and the 10 channels of the local shear strains, displacement and shear load were also digitally recorded.

3. Experimental Results

3.1. Coseismic Electric Signal

Figure 2 shows a typical record of shear load and electric potential differences associated with an unstable slip event for a slip of approximately 80×10^{-6} m. We detected coseismic electric potential signals the moment slip occurs with a sudden stress drop. The coseismic signals start like a spike, with amplitudes of about 1.5 V, and then decay exponentially. We also detected preseismic signals. Enlargement of the y axes of Figures 2b and 2c produces Figures 2d and 2e, respectively, denoting a preseismic signal just before the rupture with an amplitude of about 50 mV at electrode EL1. In the present series of experiments, the coseismic and preseismic signals were always detected whenever unstable slip occurred. The signs of the coseismic signals were positive for EL1 and negative for EL3 without exceptions. If net charges had been generated in

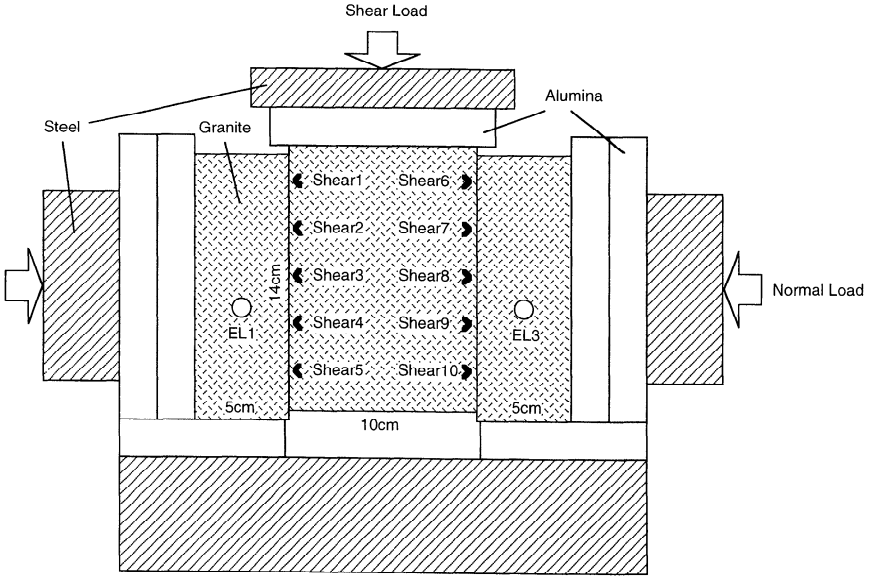

Figure 1. Diagram of the sample assembly. The dimension of the sliding surface is approximately 14 cm × 5 cm. The granite blocks are electrically isolated by alumina blocks from the ground. The silver electrodes are mounted on the reverse side of the outer blocks.

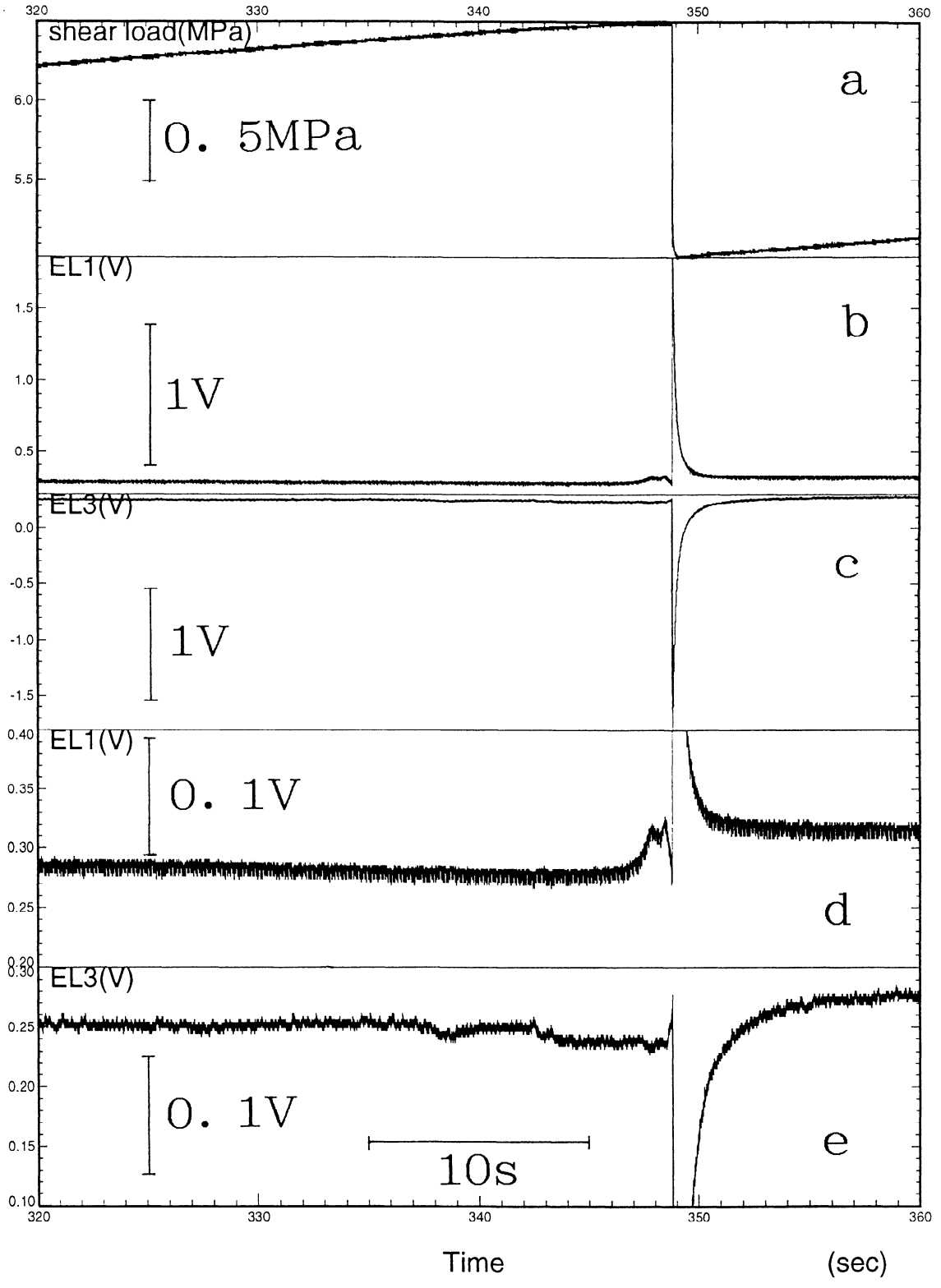

Figure 2. A typical record of the observed electric potential changes associated with stick-slip instability in the granite sample at a normal stress of 8 MPa. (a) When a dynamic event occurs with a rapid stress drop, electric potential changes are detected at electrodes (b) EL1 and (c) EL3, which have opposite polarities of signals each other. (d) and (e) Two traces with enlarged y axes show that a preseismic signal is also detected. In this example, the preseismic signal at electrode EL1 has a higher amplitude than EL3 because the rupture nucleation grows on the left sliding surface, which is close to EL1.

the rock sample, the signs would have been the same for both the electrodes. This difference in sign suggests that the coseismic signal is not due to generation of net charges but due to other mechanisms such as polarization charges. We will first consider the coseismic signals because they are much larger than the preseismic signals.

There is a possibility that the strain gauges mounted on the sample produced electric noise. To check this, we turned off the power of the bridge box connected to the strain gauges and found no differences in the electric potential records. The feature of the preseismic and coseismic signals was not influenced by mounting the strain gauges.

When the coseismic signals are generated, two kinds of kinetic processes are occurring at the same time, i.e., sliding and stress change. To see the effect of stress change separately from the effect of sliding, we carried out a simple test by changing stress without sliding. We applied the shear stress less than half the maximum frictional strength (about 6.5 MPa) and lowered the stress suddenly. Because the stress was lower than the frictional strength, no slip occurred. The electric signal associated with the stress drop is shown in Figure 3, which indicates almost the same signals as the coseismic ones in Figure 2. The polarity, the decay time, and the amplitude per megapascal of stress change are approximately the same. This suggests that the main mechanism of generating coseismic signal observed in our experiment is due to stress change, not due to sliding. When we suddenly increased the shear load, the polarities of the signals were reversed. Similar results have been reported by *Lockner et al.* [1986]. These features of the electric potential change would be explained by the piezoelectricity and the relaxation process described in the next section.

3.2. A Model for Generating Electric Signals Based on the Piezoelectric Effect

We propose a quantitative model describing the mechanism of generation of electric signal based on the piezoelectric effect and the succeeding relaxation process. Basically, the same idea has been described by *Yoshida et. al* [1994]. First, consider a quartz crystal in the rock which is electrically polarized in proportion to the applied stress σ_{ik}^0:

$$p_i^0 = c_{ijk}\,\sigma_{ik}^0$$

where p_i is the ith component of the polarization vector, c_{ijk} is the piezoelectric modulus of the third-order tensor. The summa-

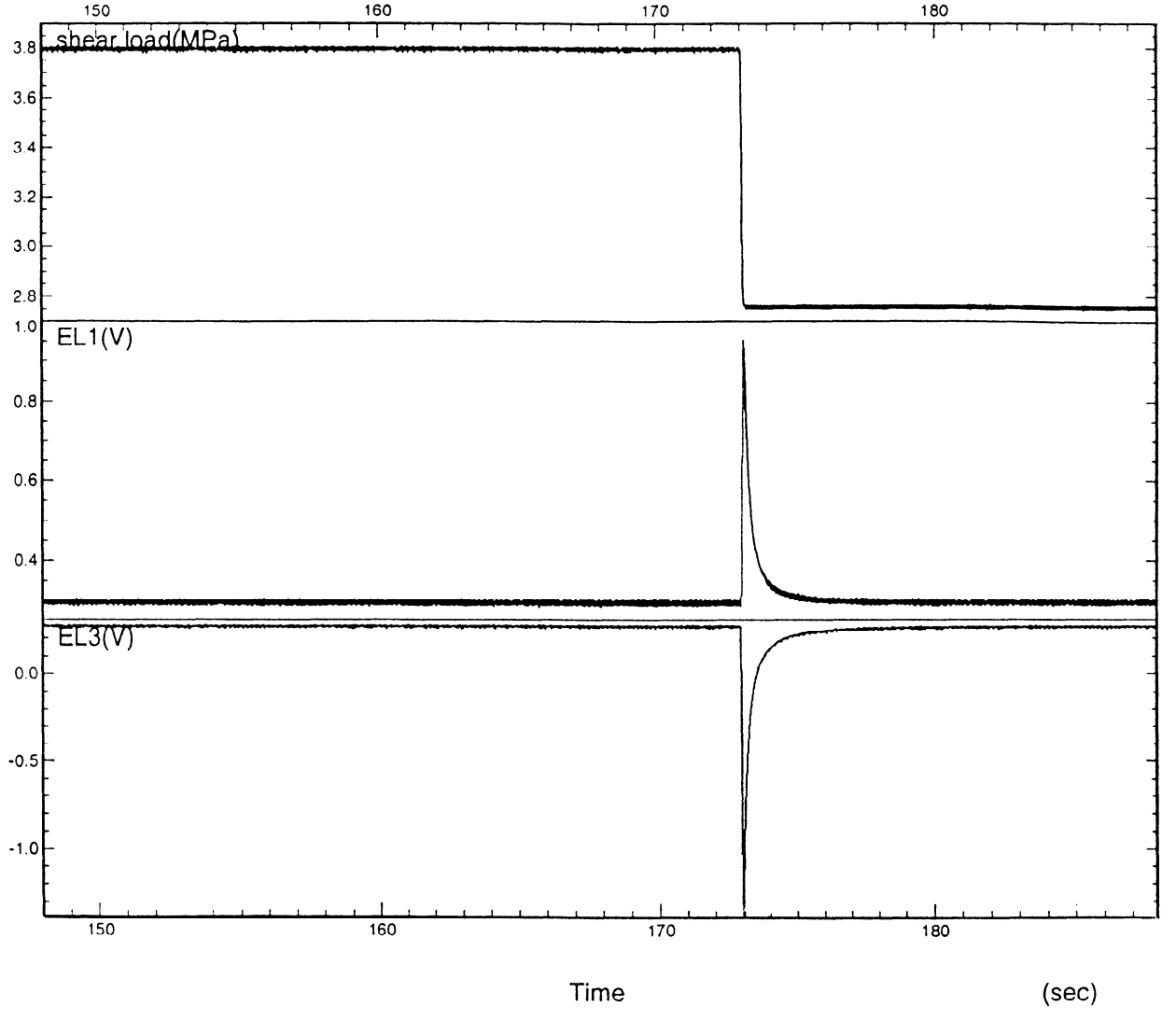

Figure 3. The electric potential changes when stress drop occurs without sliding. Almost the same signals as the coseismic signals are observed. This suggests that the stress change generates the coseismic signals.

tion convention for repeated subscripts is followed. Initially, the polarization charges are neutralized by compensating bound charges which have moved to the quartz surface (Figure 4a); consequently, the polarization cannot be detected as an electric potential signal from the outside of the rock. When a stick-slip event occurs, the quartz crystal is subjected to a rapid stress drop $\Delta\sigma_{jk}$, and the polarization of the quartz is reduced to $p_i = c_{ijk}(\sigma^0_{jk} - \Delta\sigma_{jk})$ (Figure 4b). If the stress drop occurs rapidly enough compared with the relaxation time required for the bound charges to leave, the neutralized state is broken and difference between the polarization due to the bound charges and the stress-induced piezoelectric polarization appears as an effective polarization $\hat{P}_i$, given as $\hat{P}_i = p_i - p^0{}_i = - c_{ijk}\Delta\sigma_{jk}$. The effective polarization can be seen from the outside of the rock as an electric signal, the polarity of which depends on the direction of the electrical axis of the quartz crystal. The effective polarization is followed by relaxation process (Figure 4c). The bound charges will move to cancel the effective polarization charges. It is well known that the charge density which is suddenly put in a medium with a permittivity of ε and an electric conductivity s decays exponentially with a relaxation time τ, given by

$$\tau = \varepsilon / s \tag{1}$$

Therefore the effective polarization $\hat{P}_i$ decays also with the same relaxation time τ and is expressed by a function of time as

$$\begin{aligned} \hat{P}_i(t) &= 0 && t < 0 \\ \hat{P}_i(t) &= - c_{ijk}\Delta\sigma_{jk}\exp(-t/\tau) && t \geq 0 \end{aligned} \tag{2}$$

where $t = 0$ is the time when the stress drop occurs. Equation (2) gives the response of the effective polarization of a single quartz crystal to a step change in stress. Dividing the Fourier transform of (2) for a unit amplitude of stress change by the Fourier transform of a step function $(1/i\omega)$, we can obtain the transfer function. Then the frequency response can be written as

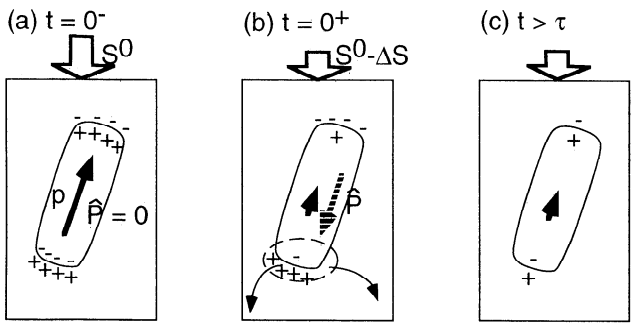

Figure 4. Schematic diagram showing a source model of electric signals based on the piezoelectric effect. (a) Initially, the stress-induced piezoelectric polarization is canceled by the compensating bound charges and rock sample is electrically neutralized. Rapid stress drop reduces the polarization of the quartz, and the neutral state is disturbed. (b) A new effective polarization due to the left bound charges appears. (c) The magnitude of the effective polarization decays exponentially with a relaxation time τ.

$$\hat{P}_i(\omega) = \frac{-i\omega}{i\omega + 1/\tau} c_{ijk}\,\sigma_{jk}(\omega) \tag{3}$$

In the time domain, we write it in the form

$$\hat{P}_i(t) = - c_{ijk}\,\sigma_{jk}(t) * g(t) \tag{4}$$

where the asterisk is a convolution operator and $g(t)$ is given by the inverse Fourier transform of $i\omega/(i\omega + 1/\tau)$. Equation (4) gives the effective polarization as a function of time for arbitrary history of applied stress. Instead of starting from the step response, another derivation of (3) can be made from the following differential equation according to *Ikeya and Takaki* [1996]:

$$d\hat{P}_i / dt = - c_{ijk}\, d\sigma_{jk}/dt - \hat{P}_i/\tau \tag{5}$$

The first term of the right-hand side means that the generation rate of the effective polarization is equal in magnitude to the disappearance rate of the piezopolarization, and the second term corresponds to relaxation due to the decay of the bound changes. From the Fourier transform of (5), (3) is obtained.

The electric potential which we measured in the experiment is obtained by summing up the contribution from the effective polarizations of all the quartz crystals in the rock sample as

$$\begin{aligned} V(t) &= \frac{1}{4\pi\varepsilon}\sum_m \frac{v^{(m)}\hat{\mathbf{P}}^{(m)}(t)\cdot\mathbf{r}^{(m)}}{|\mathbf{r}^{(m)}|^3} \\ &= \frac{1}{4\pi\varepsilon}\sum_m \frac{v^{(m)}\hat{P}_i^{(m)}(t)\, r_i^{(m)}}{|\mathbf{r}^{(m)}|^3} \end{aligned} \tag{6}$$

where the superscript (m) means quantity of the mth quartz crystal, $\mathbf{r}^{(m)}$ is the vector from the mth quartz crystal to the observation point, and $v^{(m)}$ is a volume of the mth crystal. Here it is assumed that the polarization is homogeneous within a single crystal. Inserting (4) into (6), we obtain

$$V(t) = \frac{1}{4\pi\varepsilon}\sum_m \frac{- v^{(m)} r_i^{(m)} c_{ijk}^{(m)} \sigma_{jk}^{(m)}(t) * g(t)}{|\mathbf{r}^{(m)}|^3} \tag{7}$$

Equation (7) gives a general representation of the electric potential change due to the piezoelectric effect of the crystals, each of which is subjected to stress change $\sigma^{(m)}{}_{jk}(t)$. It can be shown that the sign of the electric potential depends on observation points.

When the whole rock deforms simultaneously, the stress $\sigma^{(m)}{}_{jk}(t)$ applied to each crystal will be proportional to shear load change $S(t)$, and we can write $\sigma^{(m)}{}_{jk}(t) = u^{(m)}{}_{jk}\,S(t)$, where $u^{(m)}{}_{jk}$ is a nondimensional proportional constant specifying the stress distribution. During the dynamic rupture event, $u^{(m)}{}_{jk}$ can be treated as a time independent constant for the first-order approximation. Then we can write

$$V(t) = \frac{1}{4\pi\varepsilon}\sum_m \frac{- v^{(m)} r_i^{(m)} c_{ijk}^{(m)} u_{jk}^{(m)}}{|\mathbf{r}^{(m)}|^3}\, S(t) * g(t) \tag{8}$$

The Fourier transform of (8) gives

$$\begin{aligned} V(\omega) &= \frac{1}{4\pi\varepsilon}\sum_m \frac{- v^{(m)} r_i^{(m)} c_{ijk}^{(m)} u_{jk}^{(m)}}{|\mathbf{r}^{(m)}|^3}\, S(\omega)\frac{i\omega}{i\omega + 1/\tau} \\ &= A\, S(\omega)\frac{i\omega}{i\omega + 1/\tau} \end{aligned} \tag{9}$$

where we replace the factor independent of ω by A in the last expression, which is a function of the crystal distribution and

the observation position. Except for A, equation (9) includes only one parameter, τ, which is of the order of 0.1 s for dry granite. If we assume a relative permittivity of $\varepsilon_r = 8$ for normal granite and $s = 3 \times 10^{-10}\ \Omega^{-1}\ m^{-1}$, which was obtained by the measurement of the same kind of granite sample from Inada area, but not the same sample used in the experiments, we obtain $\tau = \varepsilon / s = \varepsilon_r \varepsilon_0 / s = 0.24 \pm 0.05$ s.

3.3. Frequency Response Against Oscillating Stress

To check this model, we experimentally examined the frequency response of the electric potential. We applied shear load oscillating in a sine wave with various frequencies and measured the amplitudes and the phases of the electric signals (Figure 5). The mean applied stress was 2.8 MPa and the peak-to-peak amplitude of the sine wave was 0.5 MPa, resulting in a maximum stress of 3.3 MPa, which was sufficiently lower than the maximum frictional strength of about 6.5 MPa. The results are shown in Figure 6, where the theoretical responses calculated from (9) with $\tau = 0.25$ s are also indicated by solid lines. The data basically agree with the theoretical line, although phases disagree at some frequencies. At period of 0.1 s, the waveform of the input load deviated from a sine wave because of limitation of controlling the loading machine. The discrepancy may also come from too much simplification of the model. For example, permittivity and conductivity depend on frequency in actual rocks [e.g., *Lockner and Byerlee,* 1985],

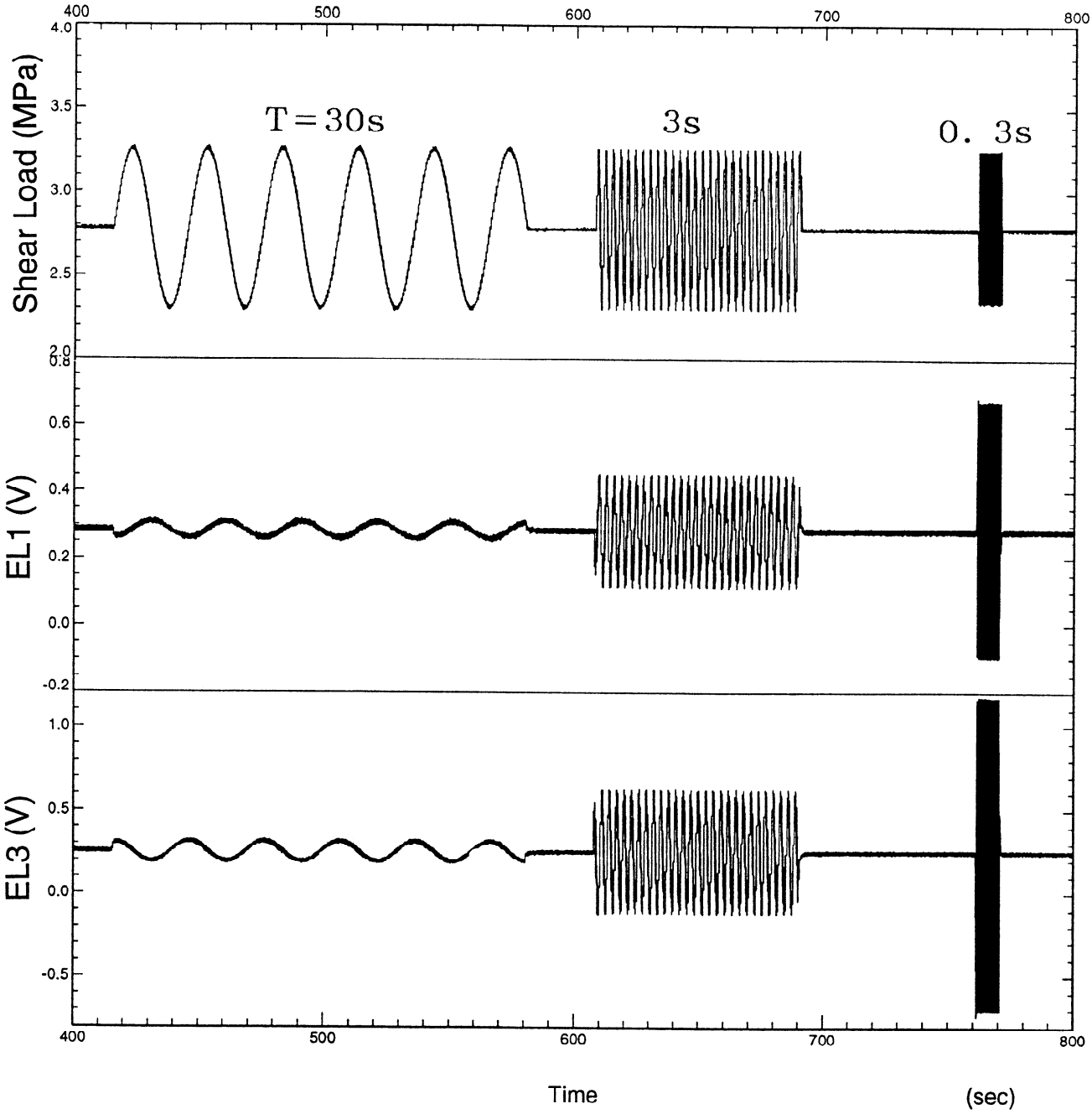

Figure 5. Electric potential changes subjected to shear load oscillating in sine waves with various frequencies. The data of the amplitudes and phases are used to determine the frequency response.

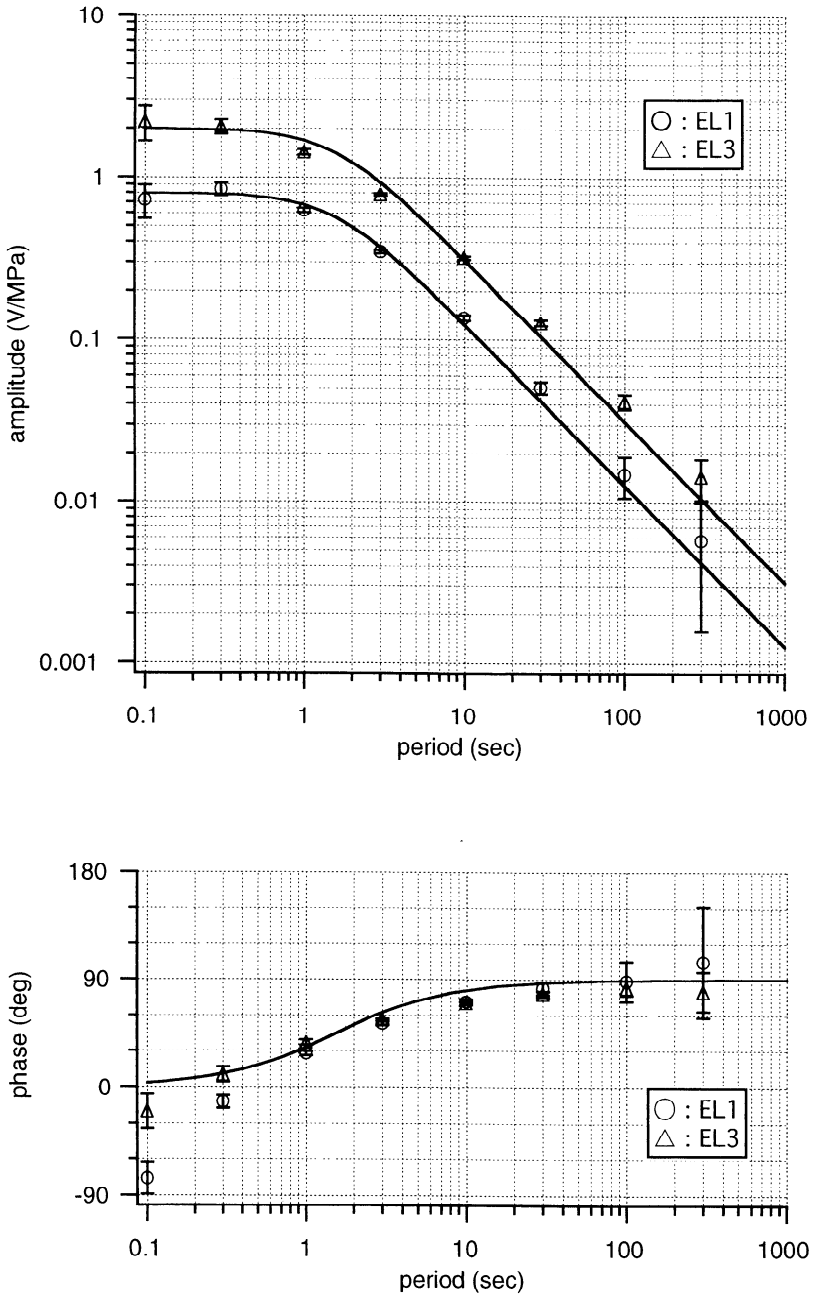

Figure 6. Comparison of theoretical and observed frequency responses of the electric potential; $\tau = 0.25$ s is assumed for calculation.

but we assume that they are constants independent of frequency. The calibration for the recording system was not made for the observation data plot. However, as the response of the recording system is almost flat for this frequency range, significant error should not occur.

Using the theoretical frequency response in (9), we can calculate the electric potential changes as a function of time for arbitrary given stress changes. Figure 7 shows the calculated electric potential for the sawtoothed type stress history with a period of 200 s, which is approximately the same as the stick-slip event experiment. The electric potential associated with the stress drop shows almost the same behavior as the coseismic signal in Figure 2. As shown in Figure 7, the electric signal for rapid stress change for which the timescale $<< \tau$ is proportional to the amount of the stress change, and for slow stress change for which the timescale $>> \tau$, this is proportional to the time derivative of the stress change. We checked these features experimentally, so validity of the response given by (9) was confirmed in the time domain as well as in the frequency domain.

For a time constant of the order of 0.1 s for the dry case, the dynamic slip is treated as a rapid phenomenon, and the generated electric signal is proportional to the stress change. However, under wet conditions, as the time constant would become of the order of 10^{-8} s for an electric conductivity of $s = 10^{-3}\ \Omega^{-1}\mathrm{m}^{-1}$, the dynamic slip is not treated as a rapid phenomenon any longer. In this case, equation (7) predicts the electric signal is proportional to the time derivative of the

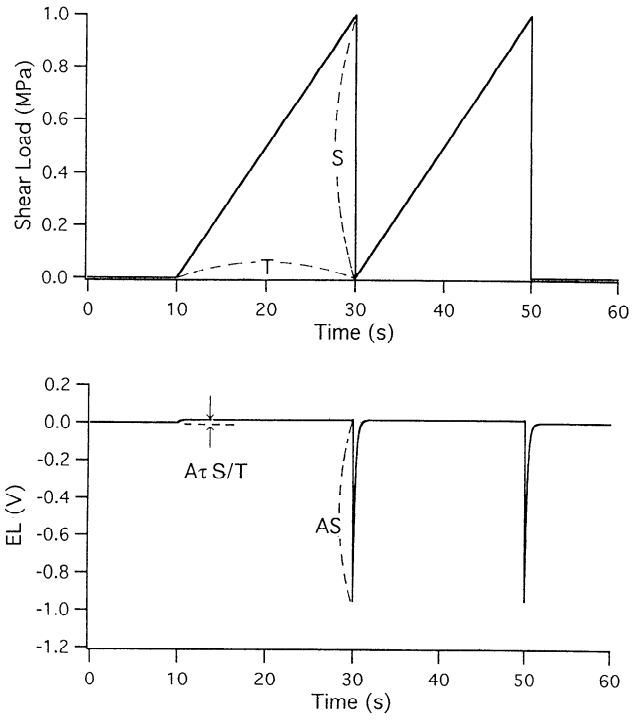

Figure 7. Calculated electric potential change for a sawtooth like change of the shear load. The response of (9) with $A = 1$ and $\tau = 0.25$ is assumed.

stress even for the dynamic event and as a result has different waveform from the dry case. An application to the actual earthquakes of this model will be considered in section 4.

3.4. Preseismic Electric Signal

Figure 2d, where the vertical axis of 2b is enlarged, shows a preseismic signal appearing about 2 s before the main rupture at the left electrode, EL1, with an amplitude of about 50 mV. A clear preseismic signal like this was always observed at both or either of the two electrodes before the repeatedly occurring dynamic slip during the experiment. The amplitude was over 200 mV at maximum. The event in Figure 2 has a clear preseismic signal at electrode EL1; the record at EL3 has only a small positive disturbance just before the onset of negative coseismic signal. Some other events, however, have a clear signal at EL3 rather than EL1. The polarity of the preseismic signal was different from event to event and was not correlated with the polarity of the coseismic one.

Laboratory experiments by *Ohnaka* [1992] showed that slip failure instability is locally preceded by a stable and quasi-static (leading to quasi-dynamic at a later time) nucleation process, if the rupture growth resistance is nonuniformly distributed on the fault. During the nucleation process, the local shear stress in the nucleation zone decreases gradually from its peak value, and at the same time the corresponding premonitory slip also proceeds. When the size of the nucleation zone reaches the critical length, dynamic instability occurs with a rapid stress drop. As mentioned before, we measured local shear strains as well as measuring the electric potential. The first five traces of Figure 8 show the strain changes on the left sliding surface, and the next five show ones on the right sliding surface. These traces denote that the local strains of ch2 to ch5 were decreasing gradually before the main rupture, which means that the rupture nucleation grows on the left sliding surface while no remarkable nucleation growth can be seen on the right-hand sliding surface. The clear preseismic signal was observed at EL1, which was located close to the left sliding surface.

During the experiment, the stick-slip event occurs repeatedly. For many events, the rupture nucleation does not grow along both the left and right surfaces at the same time. The rupture nucleation grows on the left surface for some events, like the event in Figure 8, and grows on the right-hand surface for other events. In the latter case, a significant electric potential change prior to the main rupture is observed mainly at EL3, which is mounted near the right-hand sliding surface. One of the examples in this case is shown in Figure 9. It is found that the nucleation starts from the position around ch9 and then gradually propagates. These experimental results strongly suggest that the preseismic signal is related to the nucleation process. If the preseismic signal is explained by the piezoelectric effect as well as the coseismic one, which would be a plausible assumption, the preseismic electric potential change is generated by the stress change in the nucleation zone.

Representation (7) for the electric signal can be applied to the preseismic signal as well as the coseismic signal, however, the behavior of $\sigma^{(m)}{}_{jk}(t)$ in (7) is quite different from the behavior in the coseismic case. For the coseismic deformation, $\sigma^{(m)}{}_{jk}(t)$ of all the crystals in the rock sample generate the signal at the same time, but during the nucleation process, stress change occurs only in a breakdown zone which slowly spreads. Then the onsets of appearance of the polarization effect are different from crystal to crystal. The rate of stress change is slower than in the coseismic case. As a result, the preseismic signal has a waveform different from the coseismic one. The polarity of the preseismic signal is determined by the direction of the a axis of the quartz in the nucleation zone. If the nucleation zone slightly changes in position from event to event, the polarity of the preseismic electric signal also changes, reflecting the crystal orientation in the nucleation zone. To calculate the waveform of the preseismic signal using (7), we must know the quartz distribution and local stress changes in detail. This may be difficult, but some statistical approach may be applicable, which may be a future problem.

The experimental results have shown that by observing the electric potential we can monitor the growth of the rupture nucleation as well as by observing local strains.

3.5. High-Frequency Components and Antenna Output

So far, we have examined the electric potential changes at the silver electrodes measured with the Keithley electrometers having frequency range from DC to about 100 Hz. Now we pay attention to higher-frequency components and also to the electric potential at a position away from the rock surface. To obtain broad range records, we made voltage followers which had frequency range from DC to 1 MHz and had an input impedance as high as the Keithley electrometers. To measure the electric potential outside the sample, we placed an antenna approximately 5 mm away from the rock surface of left block. The antenna is a thin plate, 45 × 45 mm, made of copper. As electric potential is usually a continuous function of position, it is expected that the signal observed at the antenna will be basically the same as the signal at electrodes mounted on the rock surface.

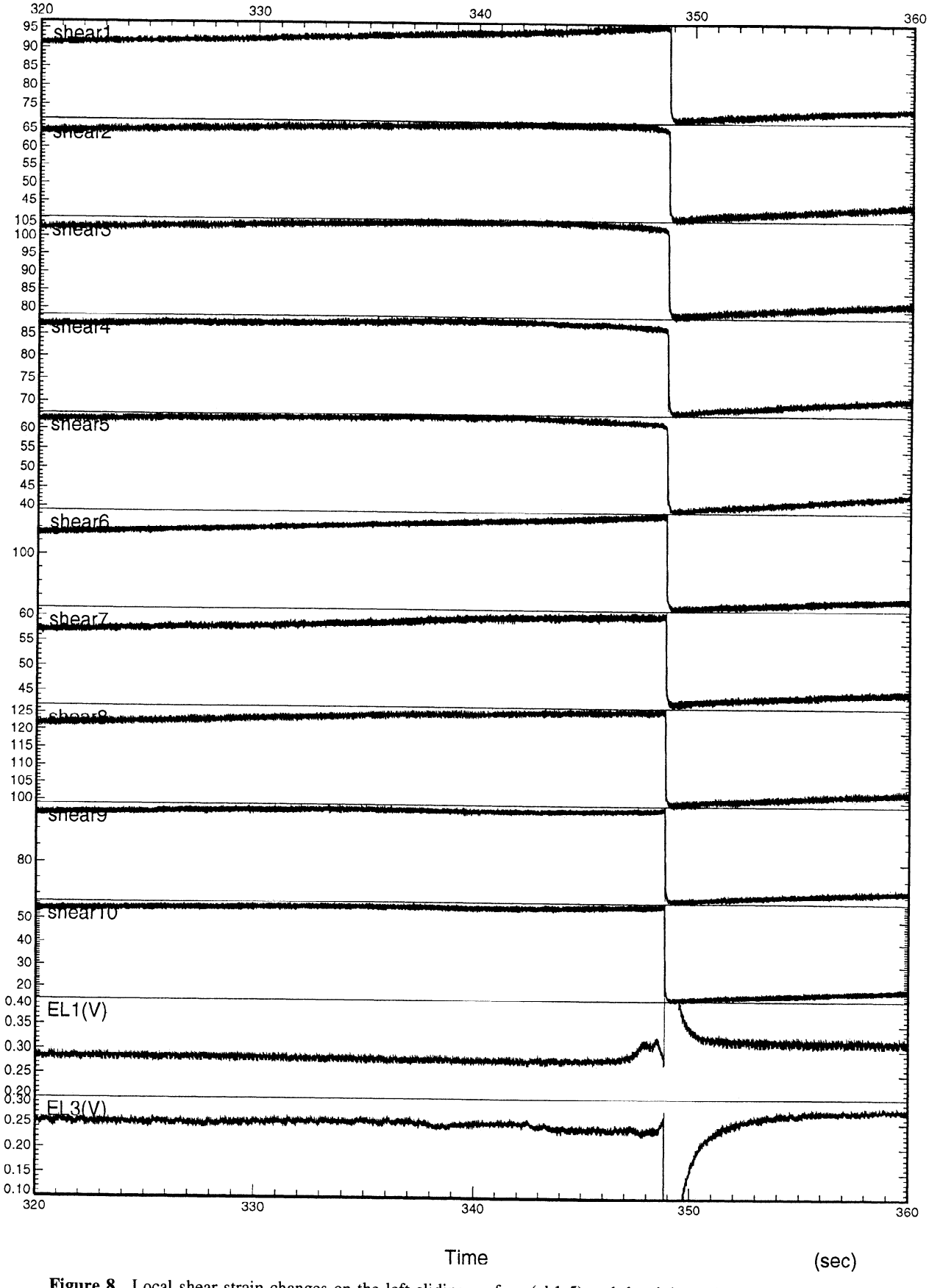

Figure 8. Local shear strain changes on the left sliding surface (ch1-5) and the right surface (ch6-10) in unit of 10^{-6} strain. The rupture nucleation is growing before the dynamic instability on the left sliding surface. The preseismic electric signal is clear at EL1 which is close to the left sliding surface. This suggests the preseismic signal is generated by the stress change in the nucleation zone.

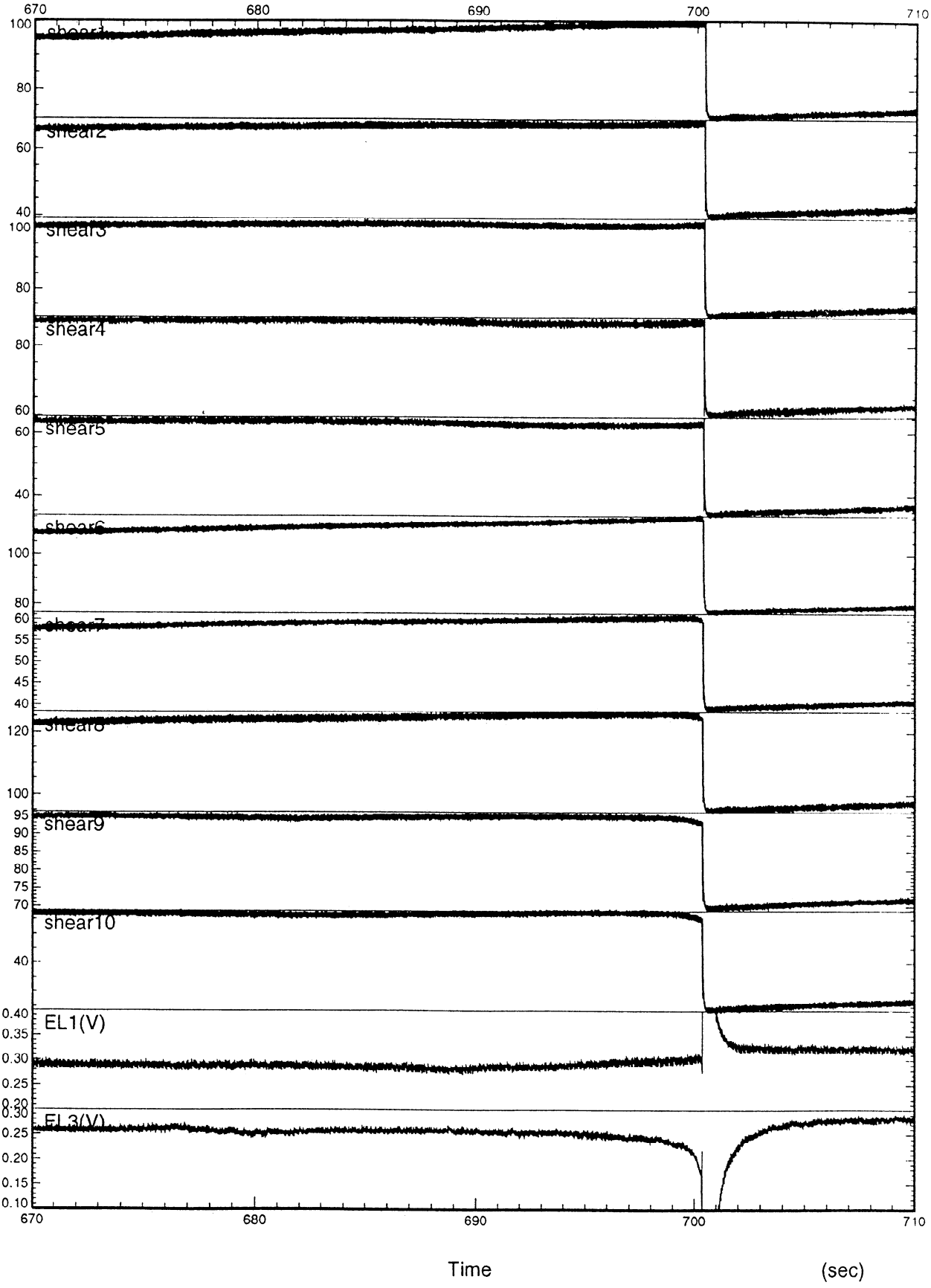

Figure 9. Shear strains and electric potential changes for another event. The rupture nucleation grows on the right-hand sliding surface, and the preseismic electric signal clearly appears at EL3, which is close to this plane.

Figure 10 shows the electric potential changes at EL1 recorded with the Keithley electrometer (Figures 10b and 10e), at EL3 with the voltage follower (Figures 10c and 10f), and at the antenna with the voltage follower (Figures 10d and 10g). Even when we measure the high-frequency components, the preseismic signal does not have high-frequency components (Figure 10f). In contrast, higher-frequency components appear with higher amplitude at the onset of the coseismic signal. The record at the antenna showed the preseismic and coseismic signals. The decay time is shorter than the electrode records, which may not mean that the true electric potential away from the rock decays quickly. Possibly, only high-pass-filtered signal of the true potential can be measured because of a capacitance between the antenna and the rock surface. Because of the high-pass-filtering effect, clear preseismic signals do not appear at the antenna for some events.

Figure 11 shows the enlarged time axis records, which is for another event, with sampling frequency of 1 MHz. Because the record was off scale, spectral analysis was not done. However, from the time domain records, we find that a number of high-frequency components (several tens of kilohertz) were included in the records at EL3 and at the antenna.

We can estimate the contribution from a single crystal subjected to a step stress change using a term in (7) for a single crystal without summation for m. If we assume a piezoelectric modules of quartz of 2×10^{-12} C/N, stress change of 1 MPa, volume of crystal of $5\times5\times5$ mm^3, and distance from the crystal to the observation point of 10 mm for a rough estimation, we obtain an amplitude of 32 V. As the observed value is > 8 V, the order estimation was not inconsistent with the observation.

The preseismic signal did not contain high-frequency components. This may reflect a general feature of the nucleation process which is a quasi-static or quasi-dynamic process [*Ohnaka,* 1992], not a dynamic one. However, it is possible that the preseismic signal has high-frequency components depending on the surface roughness. We used a sample with very smooth surfaces; therefore intense acoustic emission (AE) events did not occur during the nucleation process. If we use rough surfaces, AE will occur in the nucleation process [*Ohnaka et al.,* 1994] and a higher-frequency component of the electric signal due to AE may be observed before the dynamic rupture because AE accompanies rapid stress drop in a very localized region.

The decay time in Figure 10 was longer than that for the previous results shown in Figures 2 to 9. We conducted this experiment about 2 months after the previous experiments. As dry weather had continued in Tokyo during the period, the rock sample, without the water content being controlled, was drier than in the previous experiment, which led to a longer time constant. At the time of the previous experiments, the resistance between either of the two electrodes and an electrode mounted on the center block was about 20 GΩ, while the resistance at the time of this experiment was about 80 GΩ. Note that these values of the resistance are a combination of the surface resistivity and the bulk resistivity, so we cannot evaluate the resistivity from this measurement of the resistance between the electrodes. However, the difference in the decay time provides evidence that the decay time is strongly related to the resistivity, as suggested by our model in section 3.2.

We measured the electric potential at different distances of the antenna from the sample, up to 100 mm. Even when the antenna was located 100 mm from the sample, we detected coseismic electric signals with an amplitude of about 0.2 V, while preseismic signals were beneath the noise level.

4. Discussion

In the present work, a mechanism due to piezoelectric effect generating electric signals with DC component has been described. A number of mechanisms have been proposed by which the electric signal including electromagnetic emissions (EME) could be generated associated with rock fracture on the basis of laboratory studies. Some investigators concluded the electric signal is produced by the piezoelectric effect [e.g., *Nitsan,* 1977; *Warwick et al.,* 1982; *Ogawa et al.,* 1985; *Yoshida et al.,* 1994], but other mechanisms such as contact electrification (or separation electrification), motion of rock fragments with charged surfaces, and point defects are also proposed [e.g., *Cress et al.,* 1987; *Yamada et al.,* 1989; *Enomoto and Hashimoto,* 1992; *Hadjicontis and Mavromatou,* 1994]. However, as discussed by *Yoshida et al.* [1994], correlation between the EME amplitude and the quartz content has been observed in most of the previous works, even in the works which have disagreed with the piezoelectric effect. Although we do not object to many possible mechanisms, we believe at least in quartz-bearing rocks, the piezoelectric effect of quartz has a potential of being a major contributor to the electric signal.

Although our experiments were done under dry conditions only, the quantitative expression for the electric signal due to the piezoelectric effect obtained from the experimental result could be applied to wet rock by inserting a proper time constant into (7). Probably, the fault zones where the actual earthquake occurs are under wet conditions. For a conductivity of $10^{-3}\ \Omega^{-1}\mathrm{m}^{-1}$, the time constant becomes $\tau = 10^{-8}$ s as stated in section 3.3, which is shorter than any timescale of elastic deformation. In this case, the frequency range contained in the stress change $\sigma^{(m)}{}_{jk}(t)$ is limited to $\omega << 2\pi/\tau$, for which range the Fourier transform of $g(t)$ in (7) is equal to $i\tau\omega$. Then $g(t)$ works as a differential operator, and (7) is written as

$$V(t) = \frac{-\tau}{4\pi\varepsilon} \sum_m \frac{v^{(m)} r_i^{(m)} c_{ijk}^{(m)} \dot{\sigma}_{jk}^{(m)}(t)}{|\mathbf{r}^{(m)}|^3} \tag{10}$$

where $\dot{\sigma}_{jk}$ is a time derivative of the stress.

Now we consider how large a signal can be expected from an earthquake in the field, taking into account the randomness of the crystal distribution. Because the volume of rock in the field is much larger than in the laboratory, we need to develop a macroscopic model. Considering a volume v_0 of rock, we define the average piezoelectric modulus C_{ijk} of the rock as

$$C_{ijk} = \frac{\sum_{m \text{ in } v_0} c_{ijk}^{(m)} v^{(m)}}{v_0} \tag{11}$$

where summation is taken for the crystals in the volume of v_0. We should note that the average modulus depends on the value of v_0. One extreme situation is that all the crystals have the same axis direction; and, consequently, the same modulus $(c^{(0)}{}_{ijk})$; then the average modulus becomes

$$C_{ijk} = c_{ijk}^{(0)} \frac{\sum_{m \text{ in } v_0} v^{(m)}}{v_0} = c_{ijk}^{(0)} \frac{v_c}{v_0} \tag{12}$$

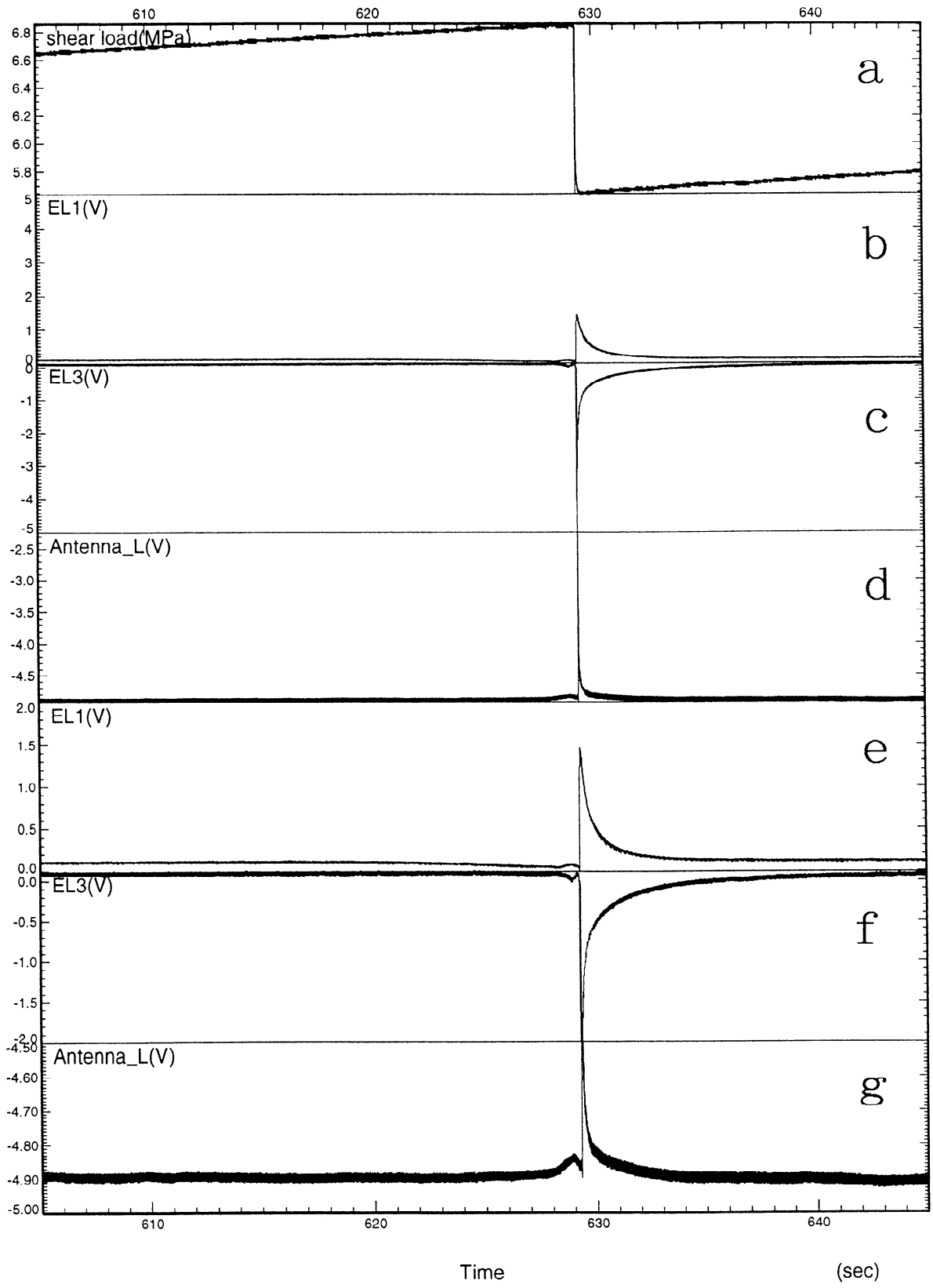

Figure 10. Electric potential changes, some of which are recorded with a measuring system with a broad frequency range (DC to 1 MHz). (a) Shear stress change, (b) electric potentials at EL1 from DC to 100 Hz, (c) at EL3 from DC to 1 MHz, and (d) at an antenna placed 5 mm away from the sample from DC to 1 MHz are shown. Traces with enlarged y axis of Figures 10b, 10c, and 10d are denoted in Figures 10e, 10f, and 10g, respectively. Preseismic signal was also detected at the antenna. The preseismic signal does not contain high-frequency components, but the coseismic signal has intense high-frequency components at the onset of the dynamic instability.

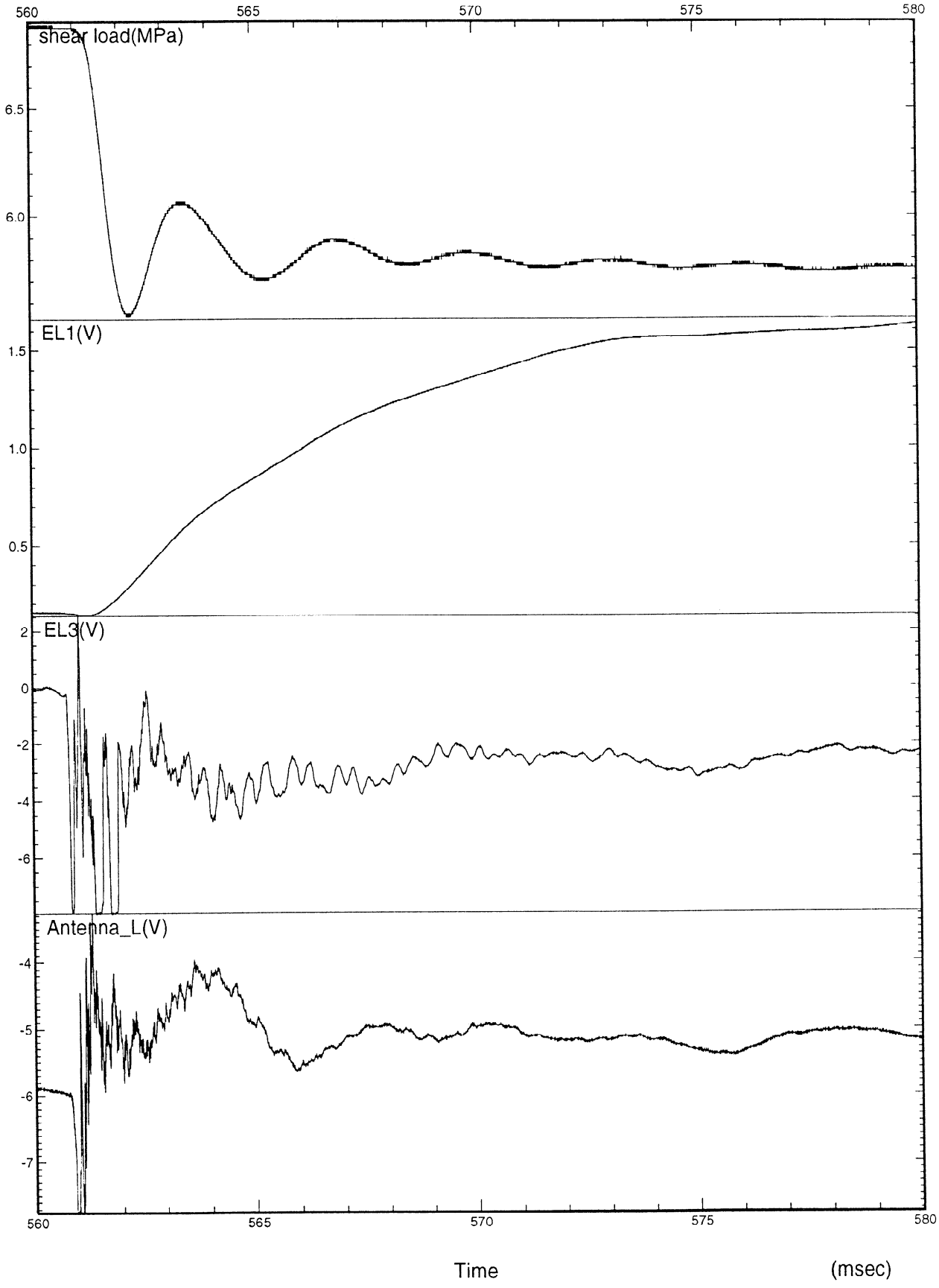

Figure 11. An example of electric signal waveforms with enlarged time axes sampled at 1 MHz using the same measuring system as Figure 10. At the onset, high-frequency (several tens of kilohertz) and high-amplitude (>8 V, off scale) signal was generated.

where v_c is the volume of the quartz crystals contained in the rock of v_0. The other extreme situation is that the distribution of the axis is perfectly random; then C_{ijk} would be nearly equal to 0 for a volume larger than a certain critical value. In general, the crystals in the rock would have an intermediate distribution between the extreme cases. For later discussion, we divide the types of the crystal distributions into the following two cases according to the degree of randomness in axis direction. When the crystal distribution is not so strongly random, $|C_{ijk}\, v_o|$ is an increasing function of v_0:

$$d|C_{ijk}\, v_o| / dv_o > 0 \tag{13}$$

For a strongly random situation, the value of $|C_{ijk}\, v_o|$ will decrease with v_0:

$$d|C_{ijk}\, v_o| / dv_o < 0 \tag{14}$$

Measured values of C_{ijk} for granite with various volumes reported by *Parkhomenko* [1971] show that both cases can occur, although the volume of the sample was limited in a small range from 10 to 500 cm^3.

Using C_{ijk}, (10) can be expressed as

$$V(t) = \frac{-\tau}{4\pi\varepsilon}\frac{r_i}{r^3}\int C_{ijk}(\mathbf{x})\, \dot{\sigma}_{jk}(\mathbf{x}, t)\, dv \tag{15}$$

Here we assumed the observation point is far from the source region and r is not dependent on the position in a source region. $C_{ijk}(\mathbf{x})$ must be evaluated in the region where $\dot{\sigma}_{jk}(\mathbf{x}, t)$ takes almost the same value. We can see that the integral in (15) has the dimension of the current dipole $I\, d_i$ and the electric potential is related to $-\tau / (4\pi\varepsilon)\, I\, d_i\, r_i / r^3 = -1 / (4\pi s)\, I\, d_i\, r_i / r^3$, which is a well-known relation for a steady state current field.

We consider one of the simplest propagating rupture models. Suppose a rectangular fault plane with length L along x axis and width W along y axis setting the z axis normal to the fault plane. The rupture initiates at one end (x=0) of the length and propagates along the length with velocity v_r. As a two-dimensional fault model with a constant stress drop [e.g., *Knopoff,* 1958] shows that the stress change is reduced to about 1/10 of the value on the fault plane at $z = W$, we will assume the thickness of the fault zone where stress change occurs is limited in $-Z/2 < z < Z/2$, with $Z/2$ of about W. Further, we assume the constant stress drop $\Delta\sigma_{jk}$ in the fault zone for simplification and describe the stress change using a ramp function of a negative polarity with a rise time of T_r:

$$\dot{\sigma}_{jk}(x, t) = h_{jk}(t - x / v_r) \tag{16}$$

with

$$h_{jk}(t) = 0 \qquad t < 0,\ t > T_r$$
$$h_{jk}(t) = -\Delta\sigma_{jk} / T_r \qquad 0 \le t \le T_r \tag{17}$$

Under this assumption, $\dot{\sigma}_{jk}$ takes the same value in the region, $v_r t - v_r T_r < x < v_r t$, $0 < y < W$, $-Z/2 < z < Z/2$, then we should evaluate C_{ijk} with (11) for the volume

$$v_0 = v_r T_r W Z \tag{18}$$

and denote the average in this region as a function of x by $C_{ijk}(x)$. The electric potential is given as

$$V(t) = \frac{-\tau}{4\pi\varepsilon}\frac{r_i}{r^3} W Z \int_0^L C_{ijk}(x)\, h_{jk}(t - x / v_r)\, dx \tag{19}$$

Putting (17) into (19), we obtain

$$V(t) = \frac{\tau}{4\pi\varepsilon}\frac{r_i}{r^3}\frac{C_{ijk}(v_r t)\Delta\sigma_{jk} v_0}{T_r}\frac{t}{T_r} \qquad 0 < t < T_r \tag{20a}$$

$$V(t) = \frac{\tau}{4\pi\varepsilon}\frac{r_i}{r^3}\frac{C_{ijk}(v_r t)\Delta\sigma_{jk} v_0}{T_r} \qquad T_r < t < L/v_r \tag{20b}$$

$$V(t) = \frac{\tau}{4\pi\varepsilon}\frac{r_i}{r^3}\frac{C_{ijk}(v_r t)\,\Delta\sigma_{jk} v_0}{T_r}\frac{(T_r + L/v_r - t)}{T_r} \qquad L/v_r < t < L/v_r + T_r \tag{20c}$$

For the case of (13), the electric signal has a higher amplitude for larger earthquakes because $C_{ijk}\, v_0$ in (20) increases. On the other hand, for the case of (14), a small earthquake can generate as high an amplitude as a large earthquake. During an actual earthquake, a large stress drop could occur in a small localized region, while this model assumed a constant stress drop. If we model a fault, dividing it into many subfaults with a different stress drop, (20) approximately gives the contribution from each subfault. A subfault with a large stress drop could generate an intense signal because the signal is proportional to the stress drop.

Equation (20) may be applied to the rupture nucleation process as a rough approximation using a very low value of v_r. If the stress change occurs very slowly during the nucleation process, the electric signal would be very small because the amplitude of the signal is proportional to τ/T_r or because the operator $g(t)$ in (6) plays as a role of strong low-cut filter. However, an unstable event can occur even during the nucleation process, as stated by *Ohnaka* [1992], for which T_r is much smaller than the averaged one over the nucleation process. As we can assume small values of W and Z for the nucleation process, resulting in a small volume of v_0, $|C_{ijk}|$ could be large in some localized regions because of less smoothing of random crystal distribution. Then relatively high amplitude electric signal due to piezoelectric effect may be generated episodically during the nucleation process. The possibility, however, seems very small that the preseismic signals are larger than the coseismic signals for the piezoelectric effect such as shown by (20). If the absence of observation of VAN signal during coseismic period is due to small amplitude, this piezoelectric model could not explain generation mechanisms of the seismic electric signals measured in the VAN method. To discuss detailed features including frequency contents, numerical simulation would be useful assuming stress change based on some physical nucleation model. Also we must obtain C_{ijk} of the rock collected from the earthquake fault zone as a function of sample volume v_0. As well as the source mechanism, propagation of the electric signal is very important in order to understand the signal observed in the field.

In the wet situation, electrokinetic effects caused by fluid flow could also generate electric signals [e.g., *Mizutani et al.,* 1976], but experimental studies on the electrokinetic effect associated with rock fracture [e.g., *Jouniaux and Pozzi,* 1995] are very few. It is necessary to perform fracture experiments in the presence of pore fluid for establishing a model related to pore fluid flow in terms of physical parameters. It is expected the frequency response is quite different from the piezoelectric mechanism because fluid cannot move as quickly. If electric signals are generated by the two mechanisms due to electrokinetic effect and piezoelectric effect at the same time in the field, we can separate such signals into the two components by combining of the model for electrokinetic effect with the result of the present study.

5. Conclusions

We measured the electric potential changes for stick-slip events in granite samples. With a three-block direct shear arrangement at 8 MPa normal stress, two electrodes EL1 and EL3 were mounted on the left- and right-hand blocks, respectively, and the electric potential difference between each electrode and the ground was measured with a frequency range from DC to 100 Hz. Both preseismic and coseismic signals were detected. We proposed a generation model based on the piezoelectric effect and the relaxation process and obtained the theorctical frequency response against stress, which was checked against the experimental data. The preseismic signal appeared about 2-3 s before the dynamic event with an amplitude of about 50 mV. The local strains measured along two sliding surfaces showed that the growth of rupture nucleation occurred on the left sliding surface when a clear preseismic signal was detected at EL1. When the growth occurred on the right-hand surface, a clear signal was detected at EL3. This shows that the preseismic electric signal is caused by the stress change in the rupture nucleation zone. These preseismic and coseismic signals were also detected with an antenna, which was placed 5 mm away from the sample surface.

Acknowledgments. We thank Hisashi Utada, Takashi Yanagidani, Osamu Nishizawa, Michiyasu Ohnaka, and Hideyuki Fujisawa for useful comments and advice, and Peter R. Sammonds for reading the manuscript and improving our English. We also thank Harmut Spetzler, Al Duba and Carl Kisslinger for their reviews and suggestions.

References

Cress, G. O., B. T. Brady, and G. A. Rowell, Sources of electromagnetic radiation from fracture of rock samples in the laboratory, *Geophys. Res. Lett., 14,* 331-334, 1987.

Dieterich, J. H., Modeling of rock friction, 2, Simulation of preseismic slip, *J. Geophys. Res., 84,* 2169-2175, 1979.

Enomoto, Y., and H. Hashimoto, Transient electrical activity accompanying rock under indentation loading, *Tectonophysics, 211,* 337-344, 1992.

Hadjicontis, V., and C. Mavromatou, Transient electric signals prior to rock failure under uniaxial compression, *Geophys. Res. Lett., 21,* 1687-1690, 1994.

Ikeya, M., and S. Takaki, Electromagnetic fault for earthquake lightning, *Jpn. J. Appl. Phys., 35,* 355-357, 1996.

Jouniaux, L., and J. P. Pozzi, Streaming potential and permeability of saturated sandstones under triaxial stress: Consequences for electrotelluric anomalies prior to earthquakes, *J. Geophys. Res., 100,* 10,197-10,209, 1995.

Knopoff, L., Energy release in earthquakes, *Geophys. J. R. Astron. Soc., 1,* 44-52, 1958.

Lockner, D. A., and J. D. Byerlee, Complex resistivity measurements of confined rock, *J. Geophys. Res., 90,* 7837-7847, 1985.

Lockner, D. A., J. D. Byerlee, V. S. Kuksenko, and A. V. Ponomarev, Stick slip, charge separation and decay, *Pure Appl. Geophys., 124,* 601-608, 1986.

Mizutani, H., T. Ishido, T. Yokokura, and S. Ohnishi, Electrokinetic phenomena associated with earthquakes, *Geophys. Res. Lett., 3,* 365-368, 1976.

Nitsan, U., Electromagnetic emission accompanying fracture of quartz-bearing rocks, *Geophys. Res. Lett., 4,* 333-336, 1977.

Ogawa, T., K. Oike, and T. Miura, Electromagnetic radiations from rocks, *J. Geophys. Res., 90,* 6245-6249, 1985.

Ohnaka, M., Earthquake source nucleation: A physical model for short-term precursors, *Tectonophysics, 211,* 149-178, 1992.

Ohnaka, M., S. Yoshida, and Shen L.-f., Slip-failure nucleation process and induced seismicity, paper presented at 27th General Assembly, Int. Assoc. of Seismol. and Phys. of the Earth's Inter., Wellington, New Zealand, 1994.

Parkhomenko, E. I., *Electrification Phenomena in Rocks*, translated by G. V. Keller, 285 pp., Plenum, New York, 1971.

Scholz, C. H., *The Mechanics of Earthquakes and Faulting,* 439 pp., Cambridge Univ. Press, New York, 1990.

Scholz, C. H., P. Molnar, and T. Johnson, Detailed studies of frictional sliding of granite and implications for earthquake mechanism, *J. Geophys Res., 77,* 6392-6406, 1972.

Shibazaki, B., and M. Matsu'ura, Spontaneous processes for nucleation, dynamic propagation, and stop of earthquake rupture, *Geophys. Res. Lett., 19,* 1189-1192, 1992.

Varotsos, P., and K. Alexopoulos, Physical properties of the variation of the electric field of the Earth preceding earthquakes, I, *Tectonophysics, 110,* 73-98, 1984a.

Varotsos, P., and K. Alexopoulos, Physical properties of the variation of the electric field of the Earth preceding earthquakes, II, Determination of epicenter and magnitude, *Tectonophysics, 110,* 99-125, 1984a.

Warwick, J. W., C. Stoker, and T. R. Meyer, Radio emission associated with rock fracture: Possible application to the great Chilean earthquake of May 22, 1960, *J. Geophys. Res., 87,* 2851-2859, 1982.

Yamada, I., K. Masuda, and H. Mizutani, Electromagnetic and acoustic emission associated with rock fracture, *Phys. Earth Planet. Inter., 57,* 157-168, 1989.

Yoshida, S., P. Manjgaladze, D. Dilpimiani, M. Ohnaka and M. Nakatani, Electromagnetic emissions associated with frictional sliding of rock, in *Electromagnetic Phenomena Related to Earthquake Prediction,* edited by M. Hayakawa and Y. Fujinawa, pp. 307-322, Terrapub, Tokyo, 1994.

M. Nakatani, Lamont-Doherty Earth Observatory of Columbia University, Rte 9W, Palisades, NY 10964, USA.

M. Uyeshima and S. Yoshida, Earthquake Research Institute, University of Tokyo, Tokyo 113, Japan. (e-mail: uyeshima@utada-sun.eri.u-tokyo.ac.jp; shingo@eri.u-tokyo.ac.jp)

(Received October 17, 1996; revised February 26, 1997; accepted March 6, 1997.)